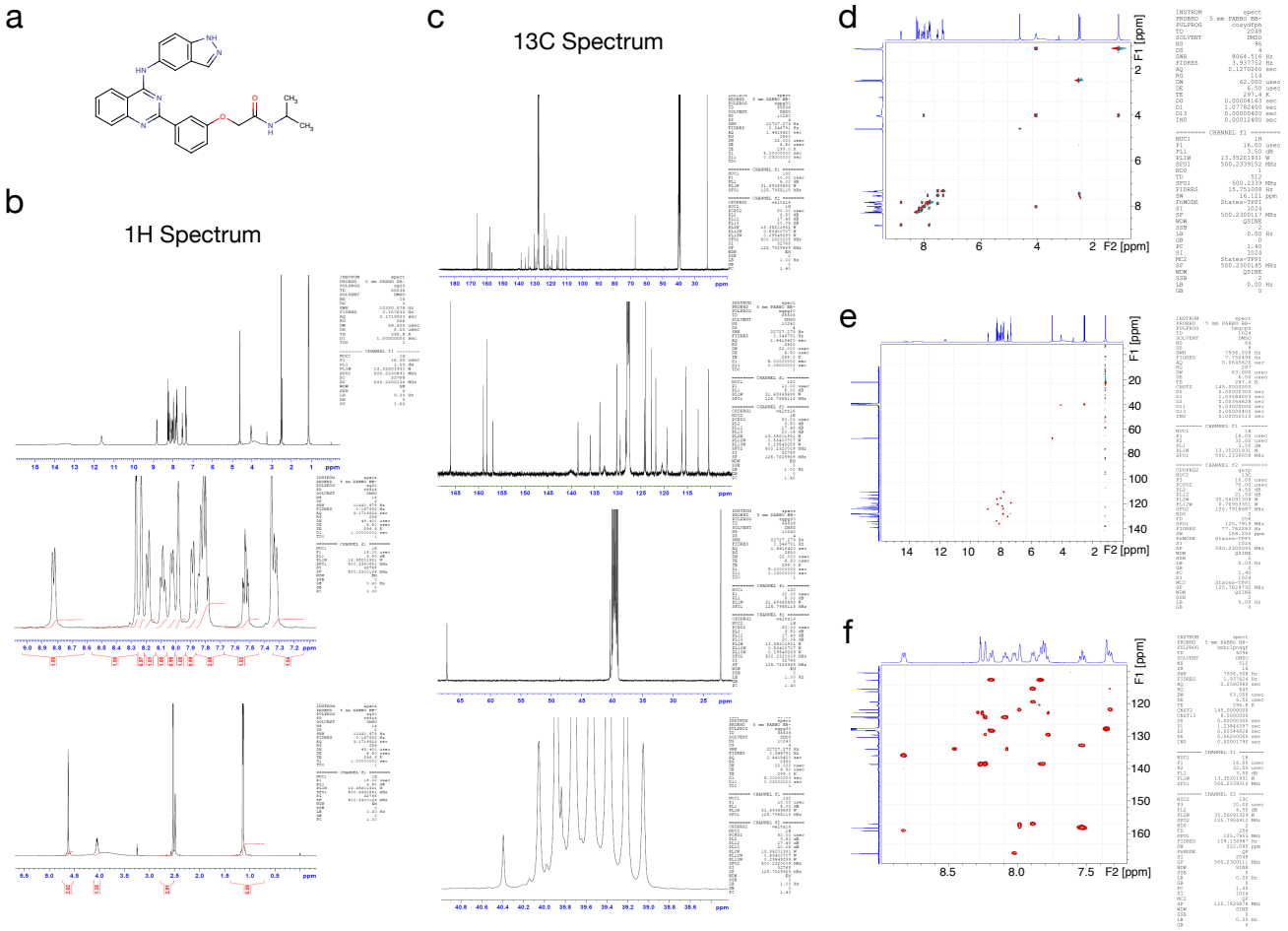

Supplemental Figure 1, related to Figure 2: Structure and nuclear magnetic resonance spectra of the ROCK2 inhibitor. (a) The selective ROCK2 inhibitor, 2-(3-(4-(1H-indazol-5-ylamino)quinazolin-2-yl)phenoxy)-N-isopropylacetamide (Sweetnam et al., 2010). **(b)** 1D 1H nuclear magnetic resonance (NMR) spectrum, **(c)** 1D 13C spectrum. **(d)** double-quantum-filtered correlation spectroscopy (COSY), **(e)** heteronuclear multiple-quantum correlation spectroscopy (HMQC), and **(f)** heteronuclear multiple-bond correlation spectroscopy (HMBC). The 1D and 2D nuclear magnetic resonance (NMR) spectroscopy results matched the properties of the ROCK2 inhibitor.

The experimental parameters are listed along with the individual spectra, where PULPROG is the pulse sequence, TD the size of the FID, NS the number of scan, SWH the spectral width, FIDRES the FID resolution, TE the temperature, and D1 the pre-scan delay. The length of the proton 90° pulse was 16 microseconds and that of 13C 10 microseconds. The spectrometer was a Bruker Avance III 500 MHz NMR system. DMSO-d6 was used as a solvent. To separate overlapping peaks in the 1-D 1H spectrum, that occasionally occur in 500 MHz NMR instruments, benzene-d6 was added drop-wise. Consequently, multiple 1-D and 2-D data sets were collected for structure determination.

a

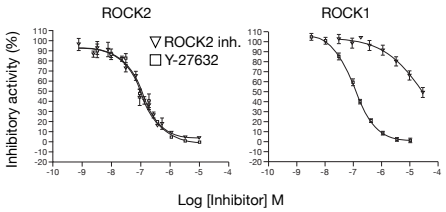

b

Ki (nM)	ROCK2 inh.	Y-27632	Fasudil
ROCK 2	41 ± 2	77 ± 5	112 ± 8
ROCK 1	> 10,000	68 ± 2	145 ± 7

c

Route	Dose (mg/kg)	C_{max} (ng/mL)	T_{max} (min)	$AUC_{0-tlast}$ (h*ng/mL)	$t_{1/2}$ (min)	Vz (L/kg)	CL (mL/min/kg)
iv	1	1620	<5	459	16	0.8	36
po	20	683	15	1359	68	14.8	1.7
po	60	3521	60	15208	253	55.2	2.3

d

Kinase	Activity (%)	IC_{50} (nM)
CK2 (h)	3	~100
Flt 3 (h)	24	5,100
MSSK1 (h)	27	>10,000
DRAK1 (h)	41	> 10,000
Ron (h)	44	>10,000
Fms (h)	46	>10,000
MuSK (h)	49	>10,000

Supplemental Figure 2, related to Figure 2: *Characterization of the ROCK2 inhibitor.* **(a)** The IC_{50} of the selective ROCK2 inhibitor and the dual ROCK1/2 inhibitor, Y-27632, for ROCK1 and ROCK2. The small molecule ROCK2 inhibitor selectively inhibited ROCK2 (IC_{50} ~105nM). In contrast to Y-27632 (IC_{50} 111nM), the ROCK2 inhibitor did not affect ROCK1 enzymatic activity at concentrations up to 10μM (IC_{50} 24μM). Briefly, recombinant ROCK1 and ROCK2 enzymes containing the truncated catalytic domains (PV3691 and PV3759) were purchased from Invitrogen and enzymatic activity was determined using [γ^{33}P]ATP (5μM) and S6 kinase substrate (17μM). The reaction was run for 45min at room temperature and was terminated by the addition of phosphoric acid. [γ^{33}P] phosphorylated S6 peptide was isolated by membrane filtration. The background was determined by running the reaction without enzyme. Radioactivity was assessed using a Microbeta Jet.

(b) Comparative enzyme inhibitor kinetics (Ki) of two existing dual ROCK1/2 inhibitors, fasudil and Y-27632 (Ishizaki et al., 2000), and the selective ROCK2 inhibitor. The selective ROCK2 inhibitor potently inhibits ROCK2, without affecting ROCK1. In comparison, Y-27632 and fasudil, showed equipotent inhibitory activities against ROCK1 and ROCK2. Therefore, in this study, the biological functions of the ROCK2 inhibitor were compared with the dual ROCK1/2 inhibitors fasudil and Y-27632.

IC_{50} was determined by curve fitting using GraphPad Prizm software (www.graphpad.com). The sigmoidal dose-response (variable slope) equation type analysis was used to generate the IC_{50} values. K_i values were calculated using the Cheng Prusoff equation of $K_i = IC_{50}/(1 + [S]/K_m)$, where [S] and K_m are the concentration of ATP and the K_m value of ATP, respectively (Lin et al., 1976).

Fasudil (HA-1077, 5-(1,4-diazepan-1-ylsulfonyl)isoquinoline hydrochloride, C14H17N3O2S.HCl, molecular weight 327.83) is in some countries an approved drug for the human use. In addition to ROCK, fasudil also inhibits, PKA, PKG, PKC, and MLCK with K_i values of 0.33μM, 1.6μM, 1.6μM, 3.3μM and 36μM, respectively.

(c) Pharmacokinetic parameters of the selective ROCK2 inhibitor. The inhibitor was administered orally (po) or intravenously (iv) at the indicated concentrations to mice and the pharmacokinetic parameters were calculated from the resulting time versus concentration curves by non-compartmental analysis using WinNonlin® (http://www.pharsight.com). T_{max}, time to reach C_{max}; C_{max}, the peak plasma concentration of the inhibitor after administration, AUC, area under the curve; $t_{1/2}$, elimination half time; Vz, volume of distribution; CL, clearance. C_{max}, $AUC_{0-tlast}$ and oral bioavailability (%F) of the ROCK2 inhibitor increased in a greater than dose responsive manner when the dose of the ROCK2 inhibitor was increased from 20mg/kg to 60mg/kg.

(d) The selectivity of the ROCK2 inhibitor was tested in the panel of over 220 representative enzymes from AGC, CMGC, TK, TKL, STE, CAMK, CK1 kinase families (KinaseProfiler™, Upstate Biology/Millipore). A small number of kinases were partially inhibited by the inhibitor at the measured 10μM concentration. IC_{50} measurements were performed for the kinases susceptible to inhibition by the ROCK2 inhibitor (IC_{50}Profiler™, Upstate Biology/Millipore). Detailed assay description, www.millipore.com/techpublications/tech1/pf3036. 'h', human,.

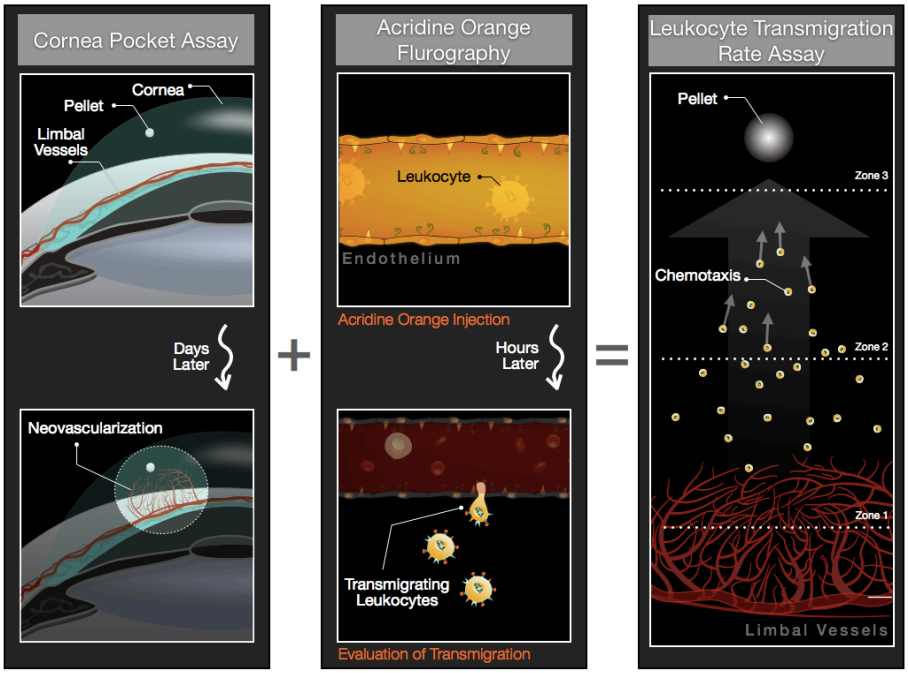

Supplemental Figure 3, related to Figure 4d: ***Model of leukocyte infiltration in the cornea.*** Schematic of our imaging technique for visualization of transmigrated leukocytes. By combining the growth factor-induced corneal angiogenesis with *in vivo* acridine orange labeling of leukocytes we developed a model, in which the leukocyte extravasation rate from limbal and angiogenic blood vessels is visualized and quantified.

Supplemental Experimental Procedure: Leukocyte transmigration assay

To visualize the leukocyte transmigration rate, we used our recently introduced assay (Nakao et al., 2012). Mice were anesthetized with ketamine (100mg/kg) and xylazine (10mg/kg). Poly-HEMA pellets (0.3µl, P3932; Sigma, St. Louis, MO, USA) containing 400ng MCP-1 (479-JE-010/CF, R&D systems) were prepared and implanted into the corneas. Cytokine pellets were positioned at ~0.8–1.0mm distance from the corneal limbus. After implantation, bacitracin ophthalmic ointment (E. Fougera & Co., Melville, NY, USA) was applied to each eye to prevent infection.

To stain the leukocytes, 500µl AO (1mg/ml) was injected intravenously. Two hours after AO injection blood vessels were stained by perfusing the animals with rhodamine-labeled concanavalin A lectin (ConA; Vector Laboratories, Burlingame, CA, USA), 10µg/ml in PBS (pH 7.4). Briefly, under deep anesthesia, the chest cavity was opened, and a 24-gauge perfusion needle was placed into the aorta. Drainage was achieved by opening the right atrium. The animals were then perfused with 10ml PBS to wash out blood cells in the vessels. After PBS perfusion, the animals were perfused with 5 ml rhodamine-labeled ConA and subsequently with 5ml PBS to remove residual unbound ConA. Immediately after perfusion, the corneas were carefully removed, and flatmounts were prepared using a mounting medium (TA-030-FM, Mountant Permafluor; Lab Vision).

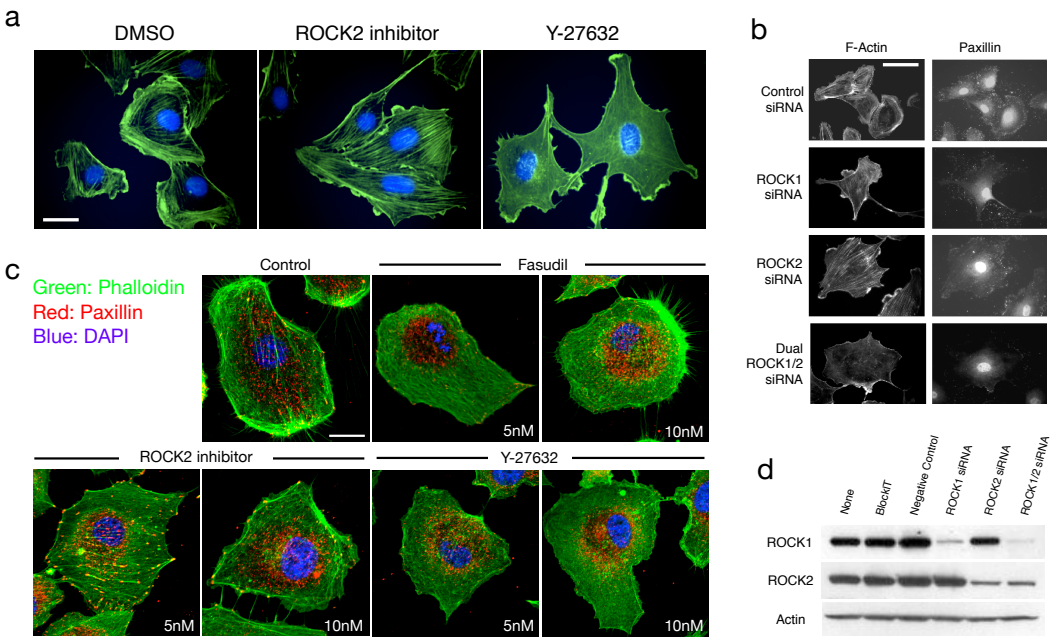

Supplemental Figure 4, related to Figure 4: ***Impact of ROCK inhibition on cytoskletal structures*****. (a)** Cytoskeletal structures of HUVECs treated with the ROCK2 inhibitor or Y-27632 at 10μM for four hours under normal culture condition. The cells were stained for actin (*green*) and nucleus (*blue*) using phalloidin and DAPI, respectively. ROCK2 inhibition does not affect the characteristic cytoskeletal structure, while dual ROCK1/2 inhibition with Y-27632 resulted in an atypically uniform cytoskeletal staining. Scale bar, 20μm. **(b)** HUVEC cells were stained for the cytoskeletal proteins F-actin and paxillin. ROCK1 blockade diminishes but ROCK2 blockade does not affect cytoskeletal structures. Scale bar, 20μm. **(c)** The effect of dual ROCK1/2 or ROCK2 inhibition on paxillin distribution was examined in cultured endothelial cells that were inhibitor treated for 30min at two different concentrations. These cells were stained for phalloidin and paxillin. In the vehicle treated controls, paxillin was distributed in the cytoplasm. When both ROCK isoforms were blocked, using the dual ROCK1/2 inhibitors fasudil or Y-27632, paxillin was no longer found evenly spread in the cytoplasm. In these cells paxillin was concentrated in the nuclear or immediate perinuclear regions. In comparison, in the ROCK2 inhibitor treated cells, paxillin distribution in the cells was comparable to the control cells. These results confirm the impact of ROCK isoform knockdowns with siRNAs. More in-depth studies of the cytoskletal changes will be required to understand the individual roles of ROCK isoforms in paxillin signaling and focal adhesion kinases. Scale bar, 20μm. **(d)** Western analysis of HUVECs transfected with siRNA targeting of ROCK1, ROCK2, or both. Negative control, a scramble 20-mer RNA. BlockIt (Invitrogen), a fluorescently labeled RNA to track uptake/transfection efficiency.

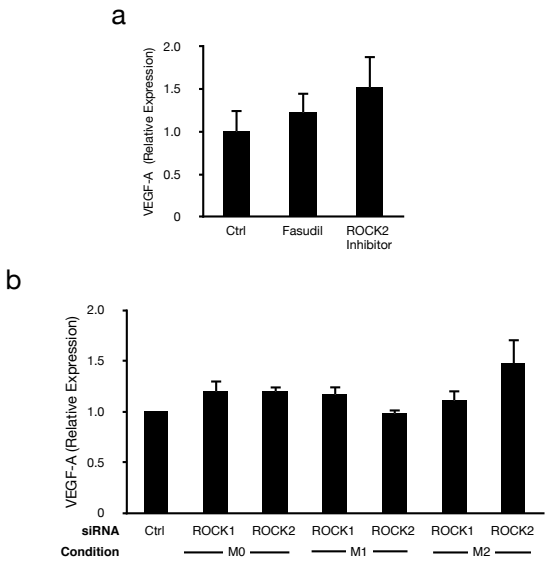

Supplemental Figure 5, related to Figure 6: ***ROCK signaling in macrophages does not affect VEGF-A expression*****.** VEGF-A is an important growth factor in AMD pathology. VEGF-A inhibition is the current standard in AMD treatment. To examine the role of ROCK signaling in VEGF-A secretion in macrophages, we measured this growth factor in cultured RAW 264.7 monocytes that were in M0, M1, and M2 state of differentiation. **(a)** Neither pharmacologic nor **(b)** gene blockade of ROCK isoforms affected VEGF-A gene or protein expression in M0, M1, or M2 macrophages. These data indicate that the anti-angiogenic and anti-leakage properties of ROCK inhibition is unrelated to VEGF-A secretion from macrophages. In line with this finding, our recent clinical data showed that ROCK inhibition ameliorates anti-VEGF resistant diabetic macular edema (DME) (Ahmadieh et al., 2013; Nourinia et al., 2013).

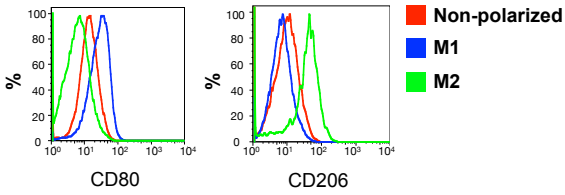

Supplemental Figure 6, related to Figure 7a: *Macrophage polarization*. For quality control, the M1 and M2 differentiated bone marrow derived macrophages were characterized by flow cytometry.

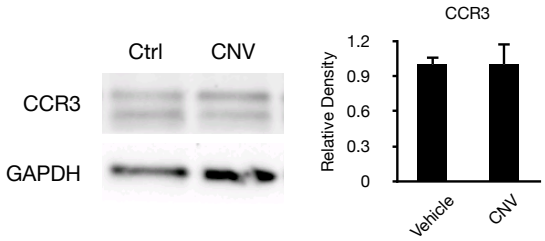

Supplemental Figure 7, related to Figure 5b & 7e: *CCR3 expression unchanged in laser-induced CNV*. CCR3 is a chemokine receptor involved in eosinophil and basophil trafficking. CCR3 is also found in TH2 cells (Sallusto et al., 1997) and is thought to take part in the type 2 response (Mantovani et al., 2004). Monocytes express CCR3, albeit at lower levels. CCR3 was reported to be elevated in CNV lesions in human AMD without any involvement of inflammation (Takeda et al., 2009). Surprisingly, our results did not show a difference in CCR3 protein expression in CNV compared to unlasered normal controls. Representative western blot from mouse choroidal tissues with and without laser injury. *n*=3 animals in each group.

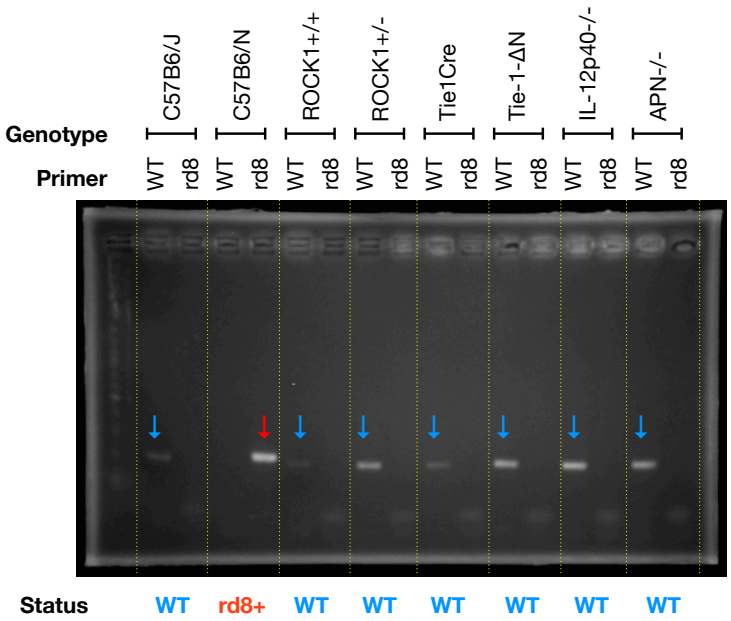

Supplemental Figure 8, related to Materials and Methods: ***Testing for the rd8 in the Crb1 gene.*** The rd8 mutation in the Crb1 gene causes retinal degeneration and AMD like features, which was previously erroneously attributed to other causes (Luhmann et al., 2013), i.e. deficiency of the Ccl2/Cx3cr1 genes (Ambati et al., 2003). Several vendor lines are contaminated with the rd8 mutation (Mattapallil et al., 2012), which made it necessary to inspect for the mutation in our experimental lines for quality control. For this purpose the PCR method, described by (Mehalow et al., 2003), was used. Representative results for each strain in our study is shown, where the size of the WT allele is 220 bp and the rd8 allele 244 bp. The results show that the mice used in our study were WT for the Crb1 gene.

Supplemental Experimental Procedure: Detection of the rd8 mutation by PCR

A fully automated nucleic acid extractor (Magtration System 6GC, PSS Co., Chiba, Japan) with a Magtration Genomic DNA Purification Kit (PSS Co.) was used to extract and purify the genomic DNA of mouse tail biopsy samples. DNA samples isolated from tail biopsies were amplified separately for wild type (WT) allele and mutant rd8 allele using primers specified by (Mehalow et al., 2003). Primer sequences included mCrb1 mF1: GTGAAGACAGCTACAGTTCTGATC; mCrb1 mF2: GCCCCTGTTTGCATGGAGGAAACTTGGAAGACAGCTACAGTTCTTCTG; and mCrb1 mR: GCCCCATTTGCACACTGATGAC. The total volume in the individual PCR assays was 40 µl, including 0.5 µl template DNA, 1.0 µl (10µM) each of forward and reverse primer for WT allele, and 1.0 µl (10µM) forward and 0.5 µl (10µM) reverse primer for rd8 mutant allele and 0.2 µl of BIOTAQTM HS DNA polymerase (BIOLINE), and 20 µl of 2×Ampdirect® Plus (Shimadzu Corp, Kyoto, Japan) containing MgCl2 (3mM) and dNTPs (400µM each). Reactions initially were denatured at 94°C for 5 minutes followed by 35 cycles at 94°C for 30 seconds, 65°C for 30 seconds, 72°C for 30 seconds and a final extension at 72°C for 7 minutes. Amplicons were separated using 3% agarose gel and visualized under UV light after staining with ethidiumbromide. Amplicon sizes are WT allele=220 bp and rd8 allele=244 bp.

Supplemental References

Ahmadieh, H., Nourinia, R., and Hafezi-Moghadam, A. (2013). Intravitreal fasudil combined with bevacizumab for persistent diabetic macular edema: a novel treatment. JAMA Ophthalmol *131*, 923-924.

Ambati, J., Anand, A., Fernandez, S., Sakurai, E., Lynn, B.C., Kuziel, W.A., Rollins, B.J., and Ambati, B.K. (2003). An animal model of age-related macular degeneration in senescent Ccl-2- or Ccr-2-deficient mice. Nat Med *9*, 1390-1397.

Ishizaki, T., Uehata, M., Tamechika, I., Keel, J., Nonomura, K., Maekawa, M., and Narumiya, S. (2000). Pharmacological properties of Y-27632, a specific inhibitor of rho-associated kinases. Mol Pharmacol *57*, 976-983.

Lin, T.S., Neenan, J.P., Cheng, Y.C., and Prusoff, W.H. (1976). Synthesis and antiviral activity of 5- and 5'-substituted thymidine analogs. J Med Chem *19*, 495-498.

Luhmann, U.F., Carvalho, L.S., Robbie, S.J., Cowing, J.A., Duran, Y., Munro, P.M., Bainbridge, J.W., and Ali, R.R. (2013). Ccl2, Cx3cr1 and Ccl2/Cx3cr1 chemokine deficiencies are not sufficient to cause age-related retinal degeneration. Exp Eye Res *107*, 80-87.

Mantovani, A., Sica, A., Sozzani, S., Allavena, P., Vecchi, A., and Locati, M. (2004). The chemokine system in diverse forms of macrophage activation and polarization. Trends Immunol *25*, 677-686.

Mattapallil, M.J., Wawrousek, E.F., Chan, C.C., Zhao, H., Roychoudhury, J., Ferguson, T.A., and Caspi, R.R. (2012). The Rd8 mutation of the Crb1 gene is present in vendor lines of C57BL/6N mice and embryonic stem cells, and confounds ocular induced mutant phenotypes. Invest Ophthalmol Vis Sci *53*, 2921-2927.

Mehalow, A.K., Kameya, S., Smith, R.S., Hawes, N.L., Denegre, J.M., Young, J.A., Bechtold, L., Haider, N.B., Tepass, U., Heckenlively, J.R*., et al.* (2003). CRB1 is essential for external limiting membrane integrity and photoreceptor morphogenesis in the mammalian retina. Hum Mol Genet *12*, 2179-2189.

Nakao, S., Zandi, S., Faez, S., Kohno, R., and Hafezi-Moghadam, A. (2012). Discontinuous LYVE-1 expression in corneal limbal lymphatics: dual function as microvalves and immunological hot spots. FASEB J *26*, 808-817.

Nourinia, R., Ahmadieh, H., Shahheidari, M.H., Zandi, S., Nakao, S., and Hafezi-Moghadam, A. (2013). Intravitreal fasudil combined with bevacizumab for treatment of refractory diabetic macular edema; a pilot study. J Ophthalmic Vis Res *8*, 337-340.

Sallusto, F., Mackay, C.R., and Lanzavecchia, A. (1997). Selective expression of the eotaxin receptor CCR3 by human T helper 2 cells. Science *277*, 2005-2007.

Sweetnam, P., Bartolozzi, A., Campbell, A., Cole, B., Foudoulakis, H., Kirk, B., Seshadri, H., and Ram, S. (2010). Rho kinase inhibitors. WO2010104851 A1.

Takeda, A., Baffi, J.Z., Kleinman, M.E., Cho, W.G., Nozaki, M., Yamada, K., Kaneko, H., Albuquerque, R.J., Dridi, S., Saito, K*., et al.* (2009). CCR3 is a target for age-related macular degeneration diagnosis and therapy. Nature *460*, 225-230.